

An Internet Database of Ultraviolet Lightcurves for Seyfert Galaxies

Jay P. Dunn^{1,2}, Brian Jackson³, Rajesh P. Deo¹, Chris Farrington¹, Varendra Das¹, & D. Michael Crenshaw¹

ABSTRACT

Using the Multimission Archives at Space Telescope (MAST), we have extracted spectra and determined continuum light curves for 175 Seyfert Galaxies that have been observed with the *International Ultraviolet Explorer (IUE)* and the Faint Object Spectrograph (FOS) on the *Hubble Space Telescope (HST)*. To obtain the light curves as a function of Julian Date, we used fix bins in the object's rest frame, and measured small regions (between 30 and 60 Å) of each spectrum's continuum flux in the range 1150 Å to 3200 Å. We provide access to the UV light curves and other basic information about the observations in tabular and graphical form via the Internet at <http://www.chara.gsu.edu/PEGA/IUE/>.

Subject headings: galaxies: Seyfert – ultraviolet: galaxies

1. Introduction

Seyfert galaxies harbor Active Galactic Nuclei (AGN) with typical redshifts $z \lesssim 0.1$ and moderate luminosities that vary over a range of time scales from days to years and over a factor of ~ 10 in amplitude. AGN have supermassive black holes consuming nearby gas and/or stars; the accretion disk surrounding the black hole is presumably the source for their high apparent luminosity and continuum variability. Seyfert galaxies are classified as types 1 and 2. Seyfert 1 galaxies have narrow (~ 500 km s⁻¹ full width half maximum [FWHM]) forbidden and permitted emission lines and broad (> 1000 km FWHM) permitted lines, while Seyfert 2 have only narrow permitted and forbidden emission lines. (Khachikian & Weedman 1974). Ultraviolet spectra of Seyfert galaxies are notable for their strong continuum variability, which is not as pronounced in the visual regime (e.g., NGC 4151, Kaspi et al. 1996).

¹Department of Physics and Astronomy, Georgia State University, Atlanta, GA 30303

²Email: dunn@chara.gsu.edu

³Lunar & Planetary Lab, University of Arizona, Tuscon, AZ 85721

The *International Ultraviolet Explorer (IUE)* began monitoring AGN in 1978 and collected a large number of UV spectra through 1995, while the Faint Object Spectrograph (FOS) on board the *HST* collected spectra from 1990 through 1997. Although the origin of the UV continuum is still elusive, it is currently believed that it is radiated from the accretion disk. Comparisons of variability in the UV with other regions of the spectrum places important constraints on the physics involved (e.g., Nandra & Papadakis 2001). Thus, it is important to have a comprehensive and uniform database of UV light curves for comparison with continuum observations at other wavelengths.

From the massive collection of *IUE* and FOS spectra, we have compiled continuum light curves and created a database that is internet accessible. Our list of targets includes any object that has been designated a Seyfert Galaxy by the observing astronomer for any observation with either *IUE* or *HST*. Also, we have limited the selection list via redshift, including only objects with a redshift $z < 0.2$. Our database is the first effort to make AGN UV light curves readily available via the World Wide Web. The only previous effort was an atlas of *IUE* spectra of Seyfert Galaxies observed prior to 1991 January 1 (Courvoisier & Paltani 1992). The database we have created is inclusive of all *IUE* and FOS spectra through their final years, and has the capability to receive further observations provided by sources such as the Goddard High Resolution Spectrograph (GHRS), Space Telescope Imaging Spectrograph (STIS), and the *Hopkins Ultraviolet Telescope (HUT)*. This information should be helpful for a number of studies, including those that require 1) the history of the UV continuum variations for an individual Seyfert galaxy, 2) a comparison of UV fluxes with measurements in other regimes of the electromagnetic spectrum for any given epoch, and 3) detailed statistical analyses (e.g., cross-correlation, structure functions) of the UV continuum properties of AGN.

2. Observations

2.1. IUE

IUE was launched on 1978 January 26 and operated successfully until 30 September 1996, when it was decommissioned. *IUE* had the capability to perform spectroscopy at two different resolutions. The high resolution mode operated at a spectral resolution of 0.1 Å to 0.3 Å (FWHM), while the low resolution mode performed at 6 Å to 7 Å (FWHM). *IUE* had two apertures available for spectroscopy: large (10 x 20 arcsec) and small (3 arcsec in diameter). Due to the faintness of Seyfert galaxies, the high-resolution mode is unsuitable for continuum studies. Observations through the small aperture are unsuitable for absolute photometry due to the large ($\sim 50\%$) and variable light loss. Thus we used only large-

aperture, low-dispersion spectra for the light curves. *IUE* utilized a total of four cameras: the Long Wavelength Prime and Redundant Cameras (LWP and LWR) and the Short Wavelength Prime and Redundant Cameras (SWP and SWR), which operated at 1850 Å to 3200 Å and 1150 Å to 2000 Å respectively. The SWR Camera was only used for a handful of observations early on, and no useful data on Seyfert galaxies were obtained. Both the LWP and LWR cameras were used to make observations over the lifetime of *IUE*. During *IUE*'s early life the LWR camera dominated the observing; during the later years the LWP camera became the dominant camera due to a flare that developed in the LWR ¹.

2.2. FOS

The FOS was one of the initial spectrographs installed on the *HST*, which was launched in 1990. It remained on board Hubble until 1997. There are two versions of the FOS data, pre-COSTAR and post-COSTAR, corresponding to data obtained before and after the optics were repaired on *HST* in 1994 January. The optics correction caused a slight change in the aperture sizes, but there were no major effects on the quality of the data. We chose to use data from all apertures, since aperture corrections for the FOS are highly reliable. The FOS had two spectral resolutions available, high ($\lambda/\Delta\lambda \sim 1300$) and low ($\lambda/\Delta\lambda \sim 250$). For our sample we chose to use the high-resolution grating due to the short exposure times and resulting poor signal-to-noise in the low resolution spectra. Although the FOS gratings covered both the UV and visible regimes, we chose to use only the UV data, from gratings G130H, G190H and G270H with wavelength ranges spanning 1000 – 1700 Å 1700 – 2200 Å and 2200 – 3000 Å respectively ².

3. Data Reduction and Analysis

For our purposes, every available spectrum was obtained using the MAST interface. The first objective was to create a single averaged spectrum per AGN from a short list of viable candidates, to identify suitable continuum regions. We chose NGC 5548, NGC 4151, Fairall 9 and Mrk 509, primarily due to their numerous *IUE* observations (367, 984, 233, and 97 observations, respectively). To view the common emission lines, the average spectra were de-redshifted and plotted together, as shown in Figures 1 and 2. We determined from the

¹See <http://archive.stsci.edu/iue/> for detailed information on the *IUE* telescope and instruments

²See <http://www.stecf.org/poa/FOS/> for detailed information on the FOS

figures where continuum flux measurements were possible with little chance of an emission or absorption line altering the flux measurements. The best locations for the SWP camera measurements fell at 1355, 1720, and 1810 Å with bin sizes of 30, 30, and 50 Å, whereas the LWP/LWR camera bins fell at 2200, 2400 and 2740 Å with bin sizes of 50, 60 and 30 Å, all in the rest frame of the galaxy. Note that fluxes in the 2200 Å bin are rather noisy compared to the other bins, due to the low sensitivities of the cameras in this region.

Our next step was to remove flawed spectra from the sample. Several reasons arose to eliminate an *IUE* spectrum from the light curve list. One such reason was overexposure. The *IUE* cameras had a limited dynamic range, such that the raw counts (in data numbers [DN]) could not exceed the value of 255. Although in most cases only the emission lines were overexposed, we decided to be cautious and not use overexposed images for our continuum measurements. Another problem that appeared was heavy background noise during periods of *IUE*'s orbit. As *IUE* orbited the Earth it would daily fall into the Van Allen belts. These events would send background counts up to high levels, thereby making the continuum fluxes very noisy. Low to moderate background values turned out to be between 50 and 100 DN, above 100 DN was considered a high value, and above 200 DN as unusable. To set a standard limit, we have omitted any spectra with background > 100 DN. During *IUE*'s later years, sunlight leaked into the telescope and added an extended source of light at wavelengths longer than 2500 Å. All spectra observed after 1990 that exhibited an unusually large increase in continuum slope in the LWR and LWP images due to this effect were excluded from our light curves. Other less prominent events affected the *IUE* spectra, but were either rare or did not affect the continuum flux. We provide in our web site a list of spectra for each object that were removed from our measurements along with a key of explanations as to what events occurred to exclude the spectra.

Once we established a quality standard, we shifted our predetermined wavelength bins by $1+z$ to measure the fluxes in the object's frame. For example, in NGC 4151 ($z = 0.0033$) the SWP bin positions shifted to 1359, 1725, and 1816 Å. When redshifting a bin near the edge of a spectrum, the 1810 bin in the SWP and the 2740 bin in the LWP camera would occasionally fall off the spectrum and yield a null result. This occurrence is the reason for a redshift limit of $z < 0.2$ in our selection list.

As discussed previously, the FOS had three fixed grating ranges available. This meant that unlike the *IUE* dataset, there was typically one bin in the G130H (the 1355 Å bin), three bins in the G190H (the 1720, 1810 and 2200 Å bins) and two bins in the G270H (the 2400 and 2740 Å bins) spectra. When examining light curves comprised of data from each source, it should be noted that the quality of spectra for measurements in the 1355 and the 1720 bins on the FOS could be vastly different, yet with *IUE* observations these two bins

were obtained at the same time and with the same camera and thus less likely to contain deviations from one another.

Once the measurements were made, we plotted the average flux in each bin versus the Julian Date of the midpoint of each exposure, calculated from the start time of the observation and the exposure length, which were taken from the file header provided by MAST. In order to extend the time span in which objects were monitored, we combined the light curves from FOS and *IUE*. An example of these results is displayed for NGC 4151 in Figure 3, along with a "zoomed in" section in Figure 4. In these light curves, it is obvious that over long time frames (years) the flux can change by a factor of 10, as previously mentioned. In Figure 4 it can be seen that small flux changes occurred over the course of three days time in the intense monitoring campaign during this time period. This is one of the few occasions in which the observations did not undersample the continuum variations (Crenshaw et al. 1996).

Continuum fluxes at the level of $\sim 2 \times 10^{-15}$ ergs s $^{-1}$ cm $^{-2}$ Å $^{-1}$ or smaller are unreliable, due to camera artifacts and uncertain background levels in the *IUE* cameras (Crenshaw et al. 1990). Note that extended continuum sources, such as starbursts or scattering regions often found in Seyfert 2 galaxies, could show apparent flux variability due to the different aperture sizes used by *IUE* and the FOS.

4. Error Analysis

In order to determine the uncertainties in the *IUE* fluxes, we began by establishing the average of the continuum in each bin, illustrated by the horizontal line in Figure 5, and then measured the standard deviation (σ) of the points within the designated bins. This method for *IUE* error determination is known to overestimate the uncertainties (Clavel et al. 1991). Because the *IUE* cameras were not photon counters and the spectra were highly oversampled, there are approximately 4 spectral points per wavelength resolution element.

For our measurements we concluded that a method of adjusting the error bars similar to the method of Clavel et al. (1991) is optimal. On time scales less than 1 – 2 days, previous studies have shown that the UV continuum variations in Seyfert galaxies are small (see Figure 4). Thus any apparent continuum variability exhibited on very short time scales in the *IUE* data is likely dominated by photon and/or instrument noise. To test this notion, we did combinatorics of all points in each light curve, for several objects that contained at least tens of observations, to find the fractional change in flux (Δf) and time (Δt) between any two points (it should be noted that this is similar to a structure function method).

Figure 6 shows a plot of Δf against (Δt) for each pair of points in Figure 3. As expected, as the time interval grows, the maximum change in flux grows. The leveling off of points on time intervals less than ~ 1 day confirms that there is no significant excess variability above the noise level (with the exception of a few points) on short time scales.

We took measurements of the light curve points contained within a rectangle between $\log(\Delta t/\text{days})$ of -1.5 and -0.5 and between $\log(\Delta f)$ of 0.0 and 0.15 in Figure 6 to characterize the noise. We define the reproducibility R as the average of the fractional variations in the time bin. R represents an upper limit to the flux uncertainty (on average), since we cannot rule out the possibility of small variations on these short time scales. The mean measured error (E_{Mean}) is given by the average of all of the uncertainties (σ) in this time interval. The overestimation of the error is given by the ratio of the mean measured error E_{Mean} and the reproducibility (R). Thus, if we divide our individual σ 's by this ratio, we obtain an estimate of the noise in each measurement, but scaled appropriately.

We repeated the above procedure for a number of well-observed Seyfert galaxies. In Tables 1, 2, and 3 we present the necessary data to determine the overestimation of the error for each camera. MaxJD and MaxFl are the logarithmic limits we imposed on the region of the plot of Δf vs. Δt to determine the reproducibility. Ratio is the average error (E_{Mean}) divided by the reproducibility (R), or, in other words, the factor by which the original errors have been overestimated. The reciprocal of the ratio averaged over all objects gives the final scaling factor for the original errors. The average ratios are 1.69 ± 0.34 , 2.40 ± 0.77 , and 1.75 ± 0.31 for the SWP, LWR, and LWP cameras respectively. For the FOS data, in the few instances where we have multiple observations of an object over short time scales, we see no evidence that the error bars require additional scaling.

5. Database and Website

We have created a web site to make our UV light curves of Seyfert galaxies available to the community. Users can access our web site at www.chara.gsu.edu/PEGA/IUE. We chose to create a MySQL database to store the data and build our web site with Perl CGI scripts. The opening page is a tabular list of the objects for which we have data, sorted by Right Ascension (see Figure 7). Users can use their web browser's "find" function to locate an object by name. The main page presents not only the list of objects and positions, but their respective redshifts and a link to the light curve for each bin that was measured (the central position of the bin is given in the observed frame). For each link, we provide an on-the-fly light curve generator (Figure 8). The user is able to adjust the time frame or the flux range within the window to allow for a zoom. For each light curve, users can left click on any point

to access the observing information for that point. We also provide a link to the information for all observations in the band pass, as well as the light curve in tabular form (Julian Date, fluxes, and scaled uncertainties) for downloading, as shown in Figure 9. This list also gives the observations that were removed from the light curve, if any. From this page, users are also able to access previews of the original spectra on the MAST web site. In the future, we hope to add points to the light curves from other UV spectrographs, such as GHRS, STIS, and *HUT*.

This research has made use of the NASA/IPAC Extragalactic Database (NED) which is operated by the Jet Propulsion Laboratory, California Institute of Technology, under contract with the National Aeronautics and Space Administration. All of the data presented in this paper were obtained from the Multimission Archive at the Space Telescope Science Institute (MAST). Support for MAST for non-HST data is provided by the NASA Office of Space Science via grant NAG5-7584 and by other grants and contracts.

REFERENCES

- Clavel, J. et al. 1991, ApJ, 366, 64
- Courvoisier, T.J.-L., & Paltani, S. 1992, IUE-ULDA Access Guide no. 4
- Crenshaw, D. M. et al. 1996, ApJ, 470, 322C
- Crenshaw, D.M., Bruegman, O.W., & Norman, D.J. 1990, PASP, 102, 463
- Kachikian & Weedman 1974, ApJ, 192, 581K
- Kaspi, S. et al. 1996, ApJ, 470, 336
- Nandra, K. & Papadakis, I.E. 2001, ApJ, 554, 710

Fig. 1.— Plots of *IUE* SWP spectra for four frequently observed Seyfert galaxies in each object’s rest frame to determine the best locations and sizes for bin measurements. These are average spectra from all of the good-quality spectra provided by MAST. The bin locations and widths used for determining the light curves are shown.

Fig. 2.— Plot of average LWP spectra for the same four Seyfert galaxies as in Figure 1. Bin locations and widths are indicated.

Fig. 3.— Example light curve plot of the 1355 bin for NGC 4151. This particular light curve shows an excellent example of large scale changes in flux over significant periods of time.

Fig. 4.— Zoomed version of Figure 3. Error bars are not shown for clarity.

Fig. 5.— Example of the 1355 bin with the SWP camera for NGC 4151, zoomed to show the average flux within the bin. The error calculated is the standard deviation of the observed points from that average flux.

Fig. 6.— Plot of the change in flux versus the change in time for NGC 4151.

Fig. 7.— Sample image of web site home page.

Fig. 8.— Sample image of the light curve on-the-fly generator.

Fig. 9.— Sample of the light curve information page.

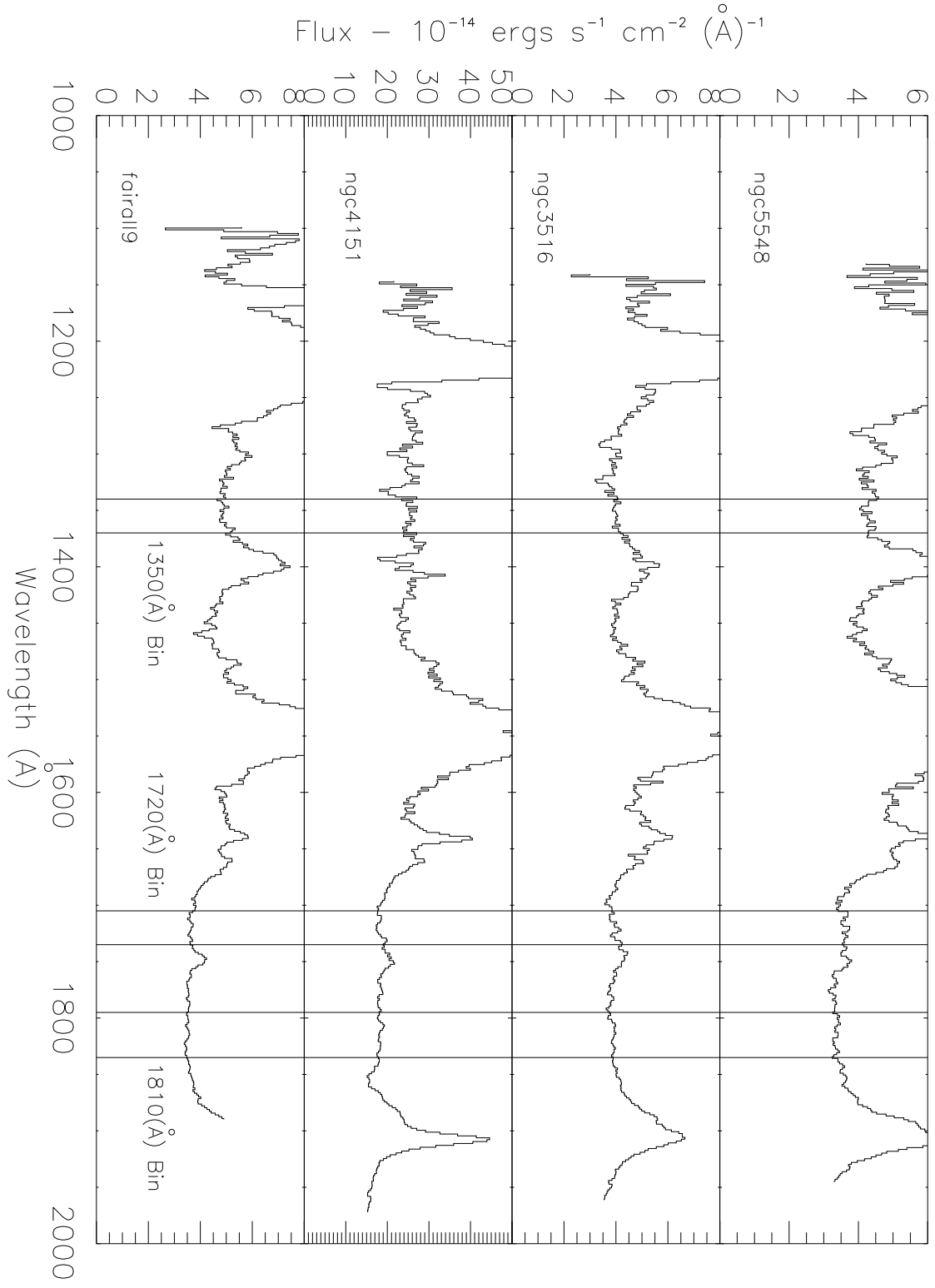


Fig. 1.

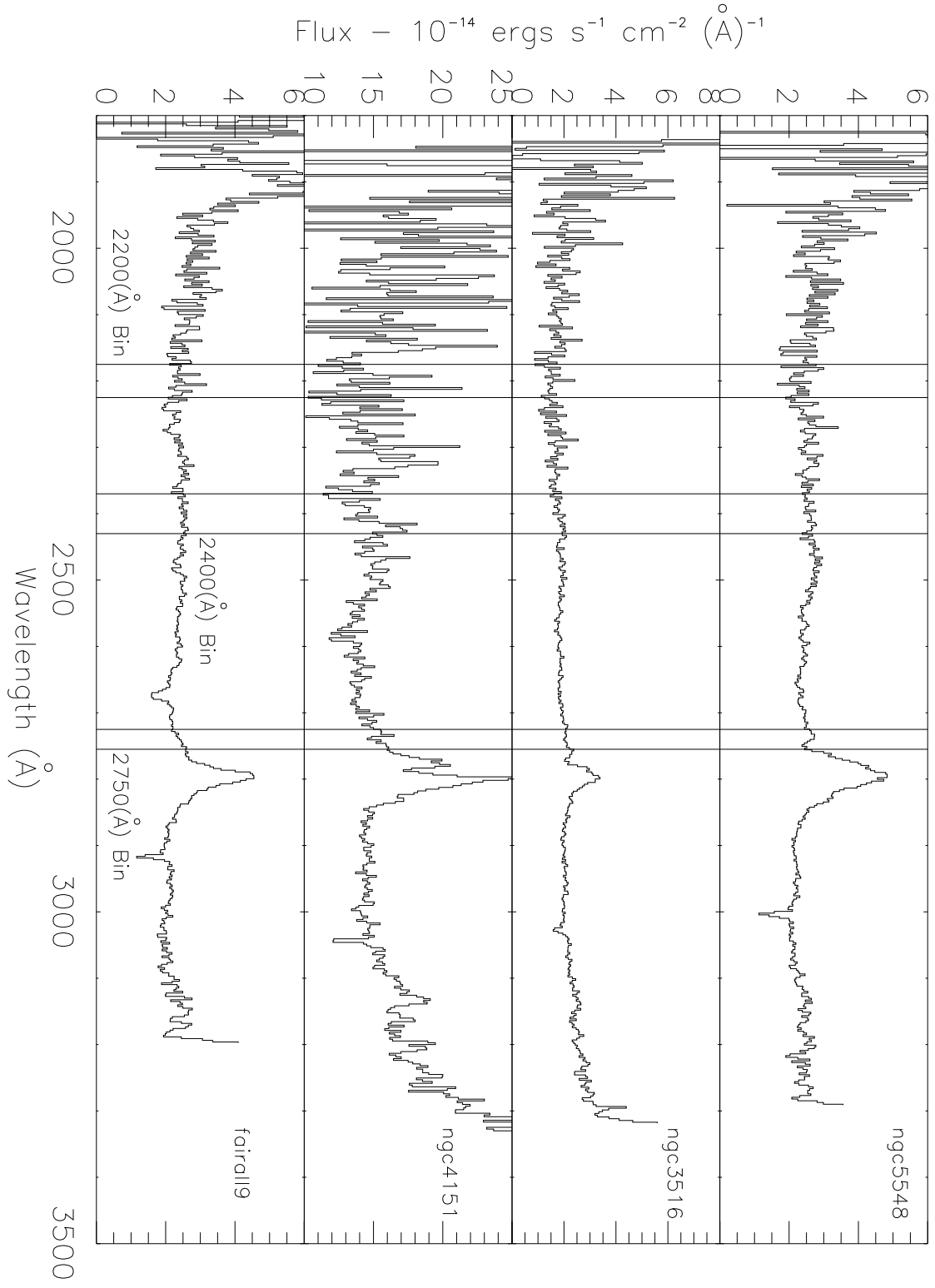


Fig. 2.

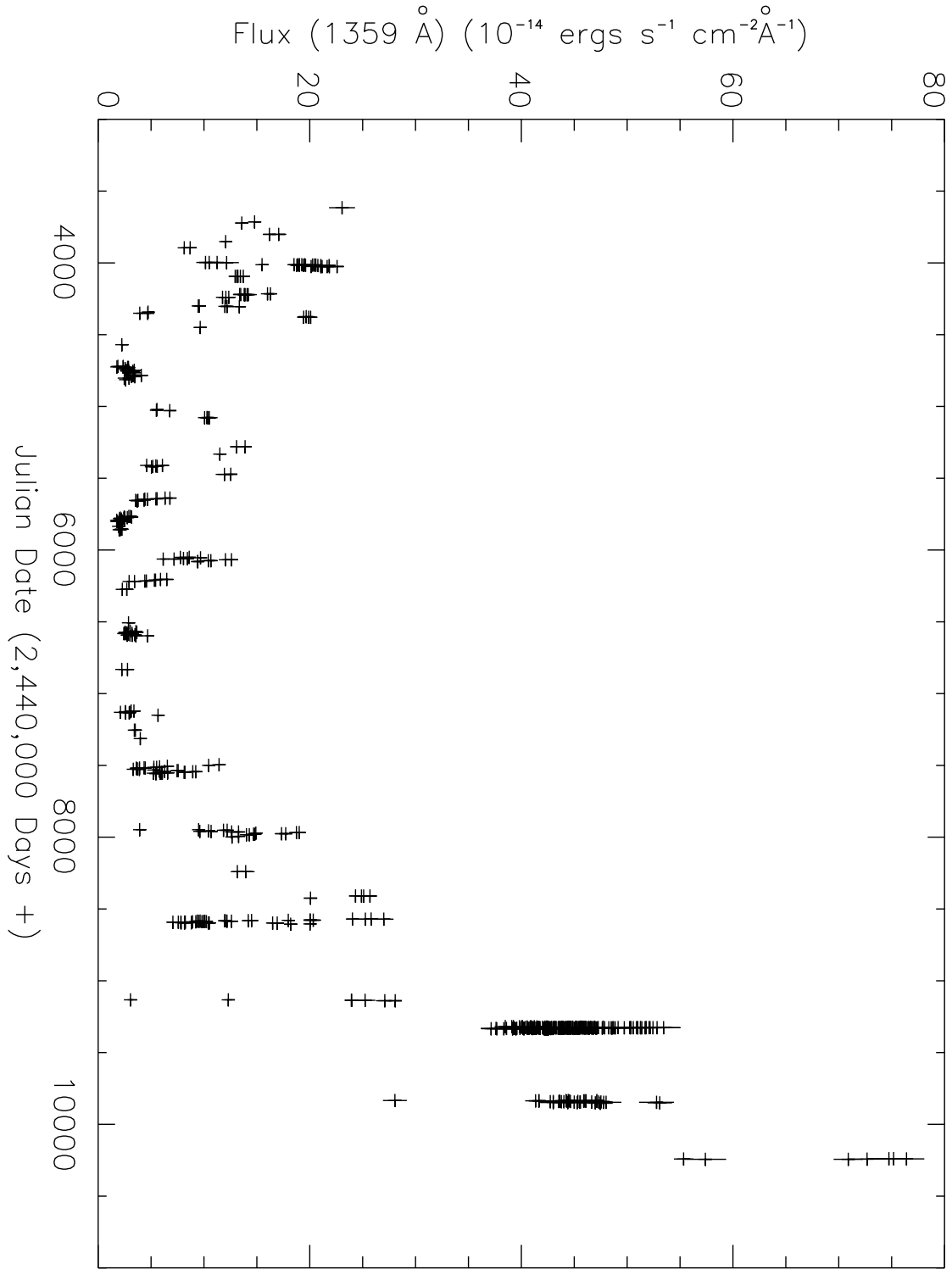


Fig. 3.

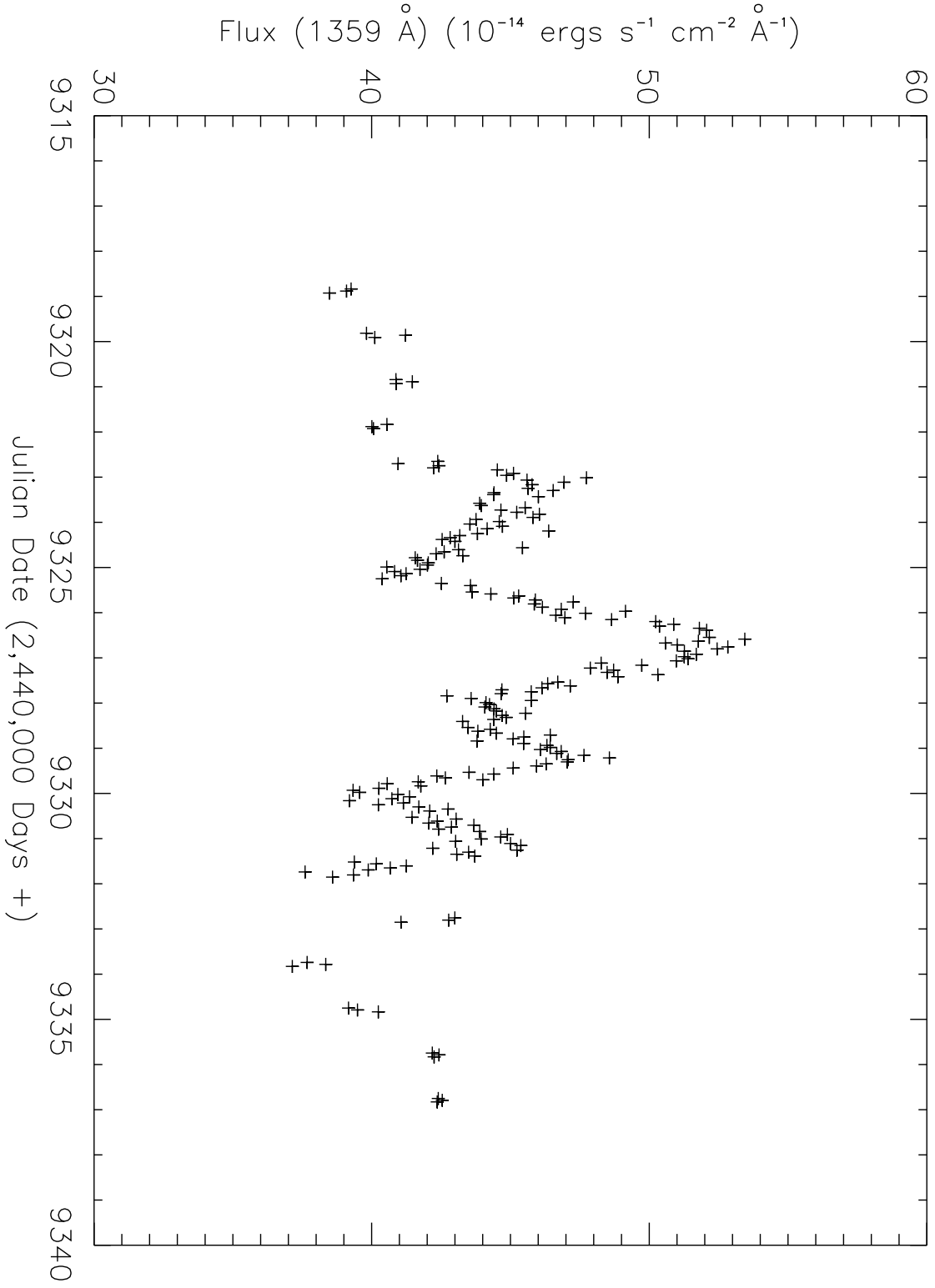


Fig. 4.

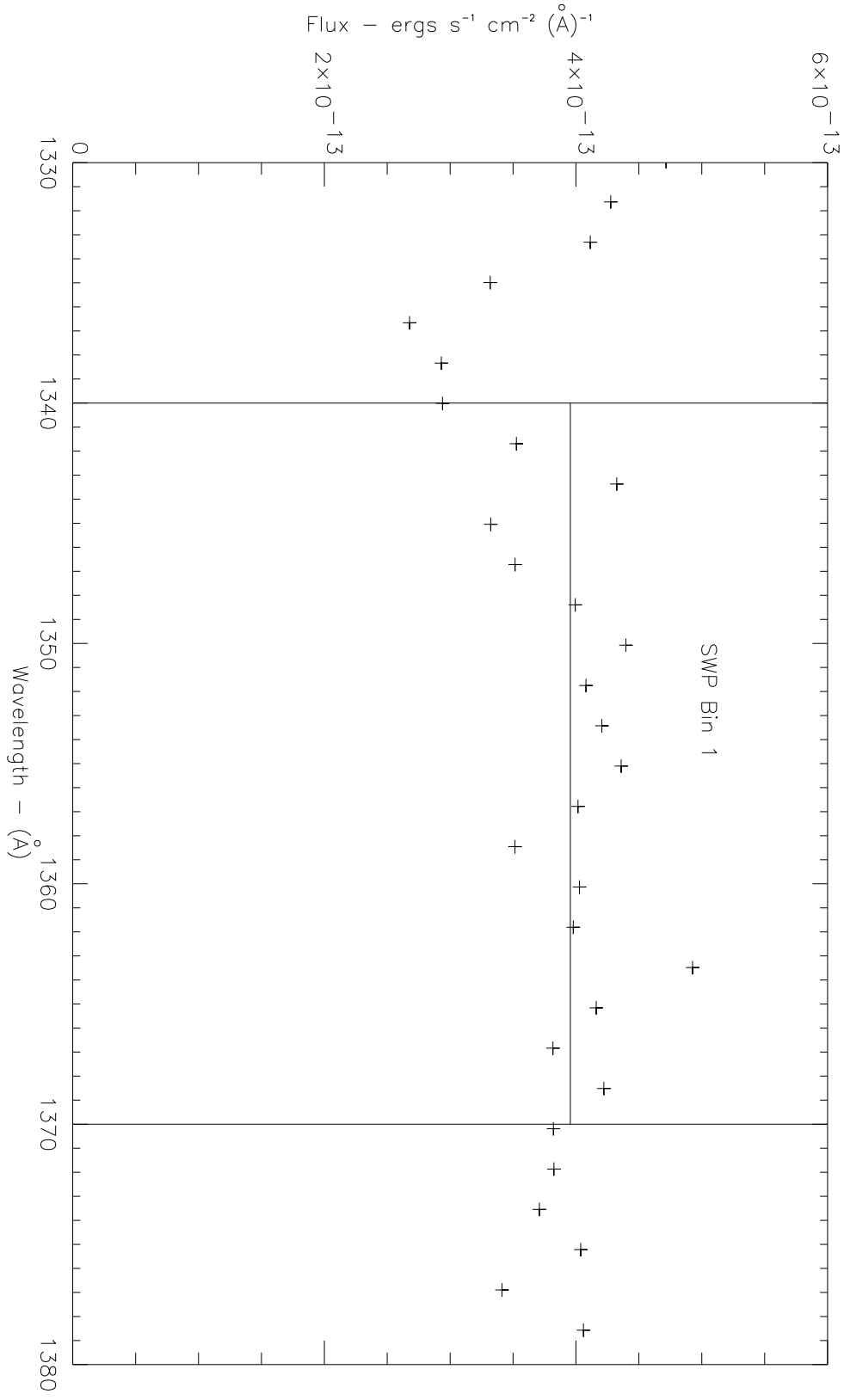


Fig. 5.

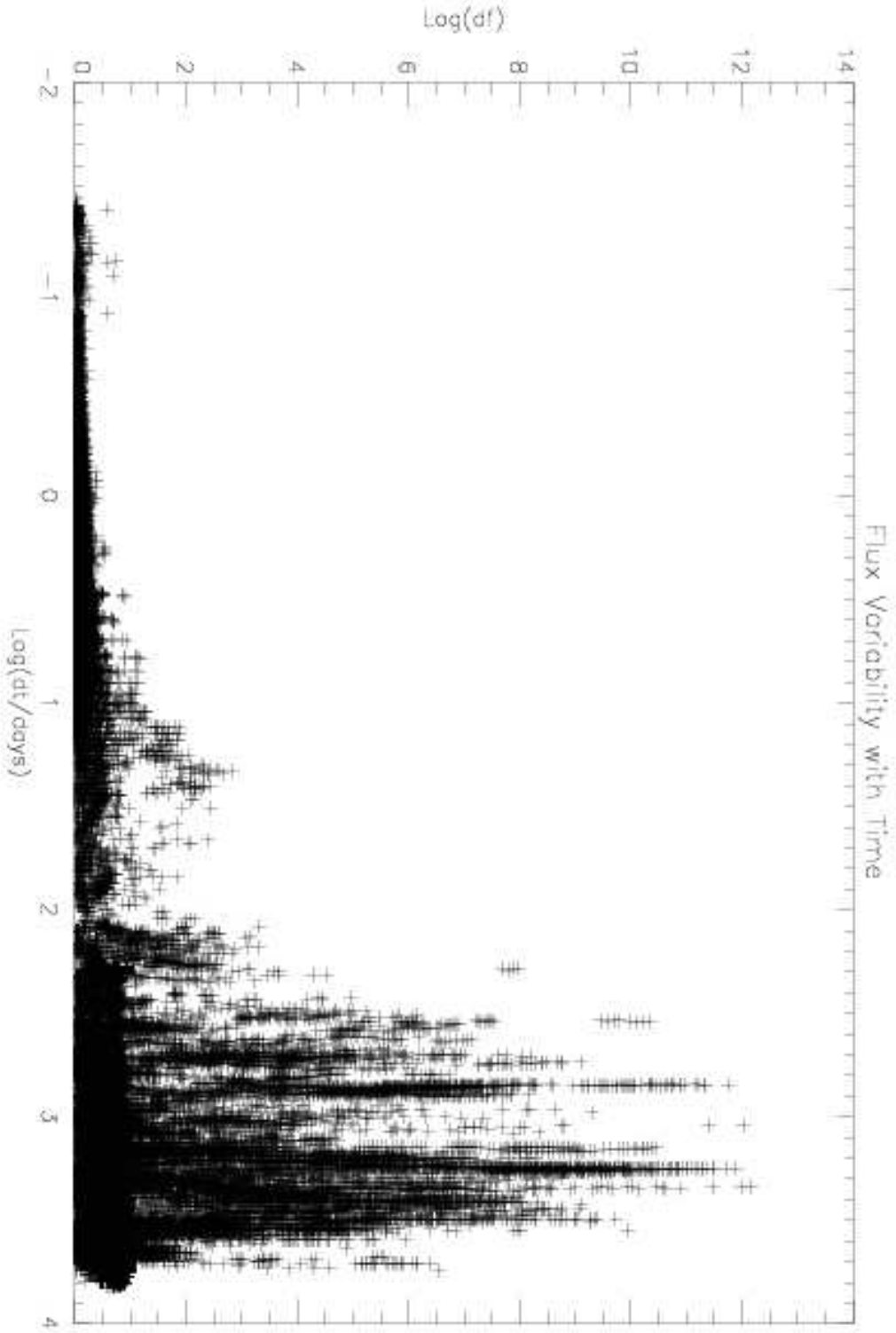
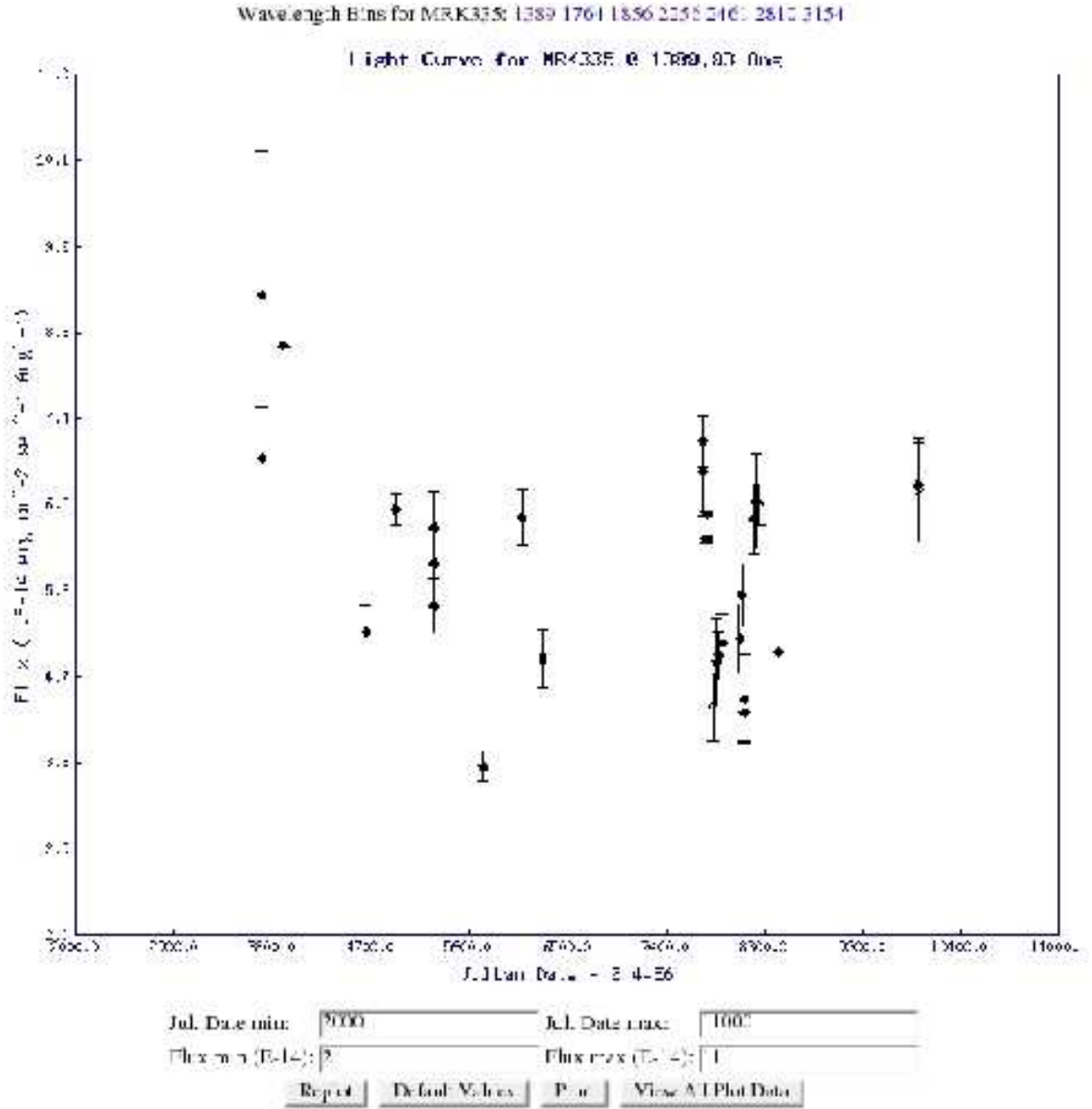


Fig. 6.

Light Curve Database: Object list sorted by RA

Object	Redshift	Right Ascension	Declination	Data Points	Redshifted Bin Wavelength
MRK335	0.02578	00 06 19.521	+20 12 10.49	165	1389 1764 1856 2256 2461 2810 3154
MRK1501	0.08934	00 10 31.005	+10 58 29.50	45	1476 1873 1971 2396 2614 2984 3349
ESO242-8	0.05604	00 25 01.28	-45 29 55.3	3	1430 1816 1911
WPV007	0.02882	00 39 15.600	-51 17 03.00	4	1394 1769 1862 2263 2469 2818 3163
IRAS00392-7930	0.03002	00 40 45	-79 14 24	6	1395 1771 1864 2266 2472 2822
MRK348	0.01503	00 48 47.144	+31 57 25.09	8	1375 1745 1837 2233 2436 2781 3121
UGC00524	0.03596	00 51 34	+29 24 06	3	2279 2486 2838
IZW1	0.00537	00 53 34	+12 41 35	39	1362 1729 1819 2211 2412 2754
TONS180	0.06198	00 57 19.944	-22 22 59.10	27	1438 1826 1922 2336 2548 2909
MRK352	0.01486	00 59 52	+31 49 39	9	1375 1745 1836 2232 2435 2780
NGC0424	0.01166	01 11 26	-38 05 00	12	1370 1740 1831 2225 2427 2771
MRK1152	0.05271	01 13 49	-14 50 44	6	1426 1810 1905 2315 2526 2884
MRK975	0.04963	01 13 51	+13 16 18	6	1422 1805 1899
MRK1	0.01595	01 16 07.249	+33 05 22.40	8	1376 1747 1838 2235 2438 2783 3124
MCT0117-2837	0.055	01 19 35	-28 21 30	3	1429 1814 1909
FAIRALL9	0.04702	01 23 45.780	-58 48 20.50	705	1418 1800 1895 2303 2512 2868 3219
MRK359	0.01739	01 27 32	+19 10 45	21	1378 1749 1841 2238 2441 2787
MICH343	0.01722	01 36 00	+00 39 47	3	1378 1749 1841
MRK573	0.01726	01 43 57.802	+02 20 59.65	8	1378 1749 1841 2237 2441 2787 3128
MCT0146-2813	0.12	01 48 22	-27 58 23	3	1517 1926 2027
MICH385	0.16301	01 59 50	+00 23 40	6	1575 2000 2105 2558 2791 3186
MRK1018	0.04244	02 06 15.990	-00 17 29.20	24	1412 1792 1886 2293 2501 2856
MRK590	0.02638	02 14 33	-00 45 59	6	1390 1765 1857 2258 2463 2812
NGC931	0.01665	02 28 14	+31 18 39	3	1377 1748 1840 2236 2439 2785

Fig. 7.



Position the mouse pointer above the plotted points to see exact data value and instrument used.

Fig. 8.

Light Curve Points for MRK335 @ 1389.93 Ang

[Back](#) to Light Curve

MAST ID	Obs. Date	Obs. Julian Date	Disp./Grating	Aperture	Right Ascension	Declination	Exposure	Instrument	Flux	Error
SWP01918	1978-07-05 15:35:00	3695.16	Low	Large	00 06 19.36	+20 12 09.01	1800.00	SWP	8.69	1.51
SWP01918	1978-07-05 15:35:00	3695.16	Low	Large	00 06 19.36	+20 12 09.01	1800.00	SWP	8.69	1.51
SWP01918	1978-07-05 15:35:00	3695.16	Low	Large	00 06 19.36	+20 12 09.01	1800.00	SWP	8.69	1.51
SWP01919	1978-07-05 17:07:00	3695.23	Low	Large	00 06 19.36	+20 12 09.01	2700.00	SWP	6.98	0.54
SWP01919	1978-07-05 17:07:00	3695.23	Low	Large	00 06 19.36	+20 12 09.01	2700.00	SWP	6.98	0.54
SWP01919	1978-07-05 17:07:00	3695.23	Low	Large	00 06 19.36	+20 12 09.01	2700.00	SWP	6.98	0.54
SWP03938	1979-01-18 13:47:00	3892.09	Low	Large	00 06 19.56	+20 12 12.01	3000.00	SWP	8.16	0.32
SWP03938	1979-01-18 13:47:00	3892.09	Low	Large	00 06 19.56	+20 12 12.01	3000.00	SWP	8.16	0.32
SWP11310	1981-02-14 23:31:00	4650.49	Low	Large	00 06 19.56	+20 12 12.01	2400.00	SWP	5.16	0.29
SWP11310	1981-02-14 23:31:00	4650.49	Low	Large	00 06 19.56	+20 12 12.01	2400.00	SWP	5.16	0.29
SWP15456	1981-11-08 21:20:00	4917.41	Low	Large	00 06 19.36	+20 12 12.01	3600.00	SWP	6.45	0.17
SWP15456	1981-11-08 21:20:00	4917.41	Low	Large	00 06 19.36	+20 12 12.01	3600.00	SWP	6.45	0.17
SWP18462	1982-11-03 13:13:00	5277.07	Low	Large	00 06 19.57	+20 12 10.93	2700.00	SWP	5.89	0.34
SWP18462	1982-11-03 13:13:00	5277.07	Low	Large	00 06 19.57	+20 12 10.93	2700.00	SWP	5.89	0.34
SWP18463	1982-11-03 16:37:00	5277.21	Low	Large	00 06 19.57	+20 12 10.93	2400.00	SWP	5.44	0.28
SWP18463	1982-11-03 16:37:00	5277.21	Low	Large	00 06 19.57	+20 12 10.93	2400.00	SWP	5.44	0.28
SWP18464	1982-11-03 19:14:00	5277.31	Low	Large	00 06 19.26	+20 12 10.94	1800.00	SWP	6.25	0.38
SWP18464	1982-11-03 19:14:00	5277.31	Low	Large	00 06 19.26	+20 12 10.94	1800.00	SWP	6.25	0.38
SWP22205	1984-02-04 22:13:00	5735.44	Low	Large	00 06 19.45	+20 12 10.01	3000.00	SWP	3.77	0.16
SWP22205	1984-02-04 22:13:00	5735.44	Low	Large	00 06 19.45	+20 12 10.01	3000.00	SWP	3.77	0.16
SWP24944	1985-01-22 00:59:00	6087.57	Low	Large	00 06 19.45	+20 12 11.01	4500.00	SWP	6.37	0.29
SWP24944	1985-01-22 00:59:00	6087.57	Low	Large	00 06 19.45	+20 12 11.01	4500.00	SWP	6.37	0.29
SWP26417	1985-07-15 09:25:00	6261.91	Low	Large	00 06 19.45	+20 12 11.01	2520.00	SWP	4.89	0.30
SWP26417	1985-07-15 09:25:00	6261.91	Low	Large	00 06 19.45	+20 12 11.01	2520.00	SWP	4.89	0.30
SWP36717	1989-07-22 08:06:00	7729.87	Low	Large	00 06 19.45	+20 12 11.01	4800.00	SWP	7.16	0.27
SWP36717	1989-07-22 08:06:00	7729.87	Low	Large	00 06 19.45	+20 12 11.01	4800.00	SWP	7.16	0.27

Fig. 9.

Table 1. Error Analysis of *IUE* data for Seyfert Galaxies (SWP)

Object	σ	Log Max JD	Log Max Fl	R	E Mean	Ratio
NGC4151	0.026	-0.50	0.15	0.032	0.067	2.06
NGC7469	0.037	-0.50	0.20	0.045	0.076	1.67
NGC3783	0.052	0.00	0.30	0.054	0.073	1.36
NGC3516	0.039	0.20	0.15	0.046	0.081	1.76
NGC5548	0.041	0.25	0.15	0.048	0.085	1.78
Fairall9	0.040	0.25	0.15	0.057	0.099	1.74
3c390.3	0.129	1.50	0.50	0.222	0.272	1.22
Mrk509	0.031	0.75	0.20	0.040	0.080	1.99
Mrk335	0.076	1.00	0.30	0.091	0.099	1.09
NGC4593	0.107	1.00	0.50	0.129	0.115	0.89
Rxj 2304.7-0841	0.096	1.50	0.50	0.114	0.150	1.32

Table 2. Error Analysis of *IUE* data for Seyfert Galaxies (LWR)

Object	σ	Log Max JD	Log Max Fl	R	E Mean	Ratio
NGC4151	0.022	-0.50	0.15	0.030	0.103	3.43
NGC7469	0.007	1.50	0.20	0.054	0.082	1.52
NGC3783	0.474	0.50	0.15	0.072	0.109	1.51
NGC3516	0.555	2.30	0.20	0.078	0.102	1.31
NGC5548	0.031	1.50	0.15	0.064	0.164	2.56
Fairall9	0.022	1.00	0.10	0.034	0.099	2.91
3c390.3	0.057	2.50	0.20	0.073	0.214	2.93
Rxj 2304.7-0841	0.032	2.00	0.20	0.037	0.111	3.00

Table 3. Error Analysis of *IUE* data for Seyfert Galaxies (LWP)

Object	σ	Log Max JD	Log Max Fl	R	E Mean	Ratio
NGC4151	0.022	-1.00	0.15	0.028	0.050	1.78
NGC3783	0.039	0.00	0.15	0.032	0.043	1.34
NGC5548	0.062	0.50	0.25	0.064	0.088	1.38
Fairall9	0.027	0.00	1.00	0.028	0.058	2.07
3c390.3	0.027	1.70	1.20	0.056	0.120	2.14
Mrk335	0.036	1.00	0.10	0.049	0.087	1.78